MECHANICS OF DEFORMABLE SOLID BODY

NUMERICAL ANALYSIS OF HIGH DENSITY ALLOYS AND ELONGATED PROJECTILES' VELOCITY AND STRENGTH EFFECT ON THEIR PENETRATION INTO A STEEL TARGET

S.V. Fedorov[1], **V.A. Veldanov**[1], **V.E. Smirnov**[2]

[1]Bauman Moscow State Technical University, Moscow, Russian Federation
e-mail: sergfed-64@mail.ru; vevladi@mail.ru

[2]Federal State-Funded Institution of Science Mechanical Engineering
Research Institute, Moscow, Russian Federation
e-mail: nimi@iplipk.ru

The paper considers the impact of velocity and material strength of the elongated projectiles made of high-density alloy on their penetration into a semi-infinite steel target. The numerical simulation of a two-dimensional axisymmetric problem of the continuum mechanics is provided. Projectile velocity is in the range from 1400 to 2000 mps and corresponds to the hydrodynamic mode of interaction with reduction of the projectile length during the penetration process as a result of its material spreading. The calculations are made with the help of the developed free Lagrangian points computational algorithm, which allows us to simulate material response under the conditions of explosive and shock loading. It was found out that dependence of the projectile penetration on the projectile material yield strength is nonmonotonic and has an extremum corresponding to penetration depth maximum. While projectile velocity is increasing the extremum is getting less defined and is shifting towards higher values of the yield strength.

Keywords: numerical simulation, elongated projectile, heavy alloy, steel target, high velocity penetration, hydrodynamic mode.

Continuum mechanics numerical methods is an effective tool for analyzing a high-velocity impact interaction of the materials [1]. This article presents the results obtained during the numerical analysis of the elongated projectile velocity and the impact of the tensile strength on high-strength steel target penetration. Calculations were considered for initial velocities in the range from 1400 mps to 2000 mps which determines a hydrodynamic mode of the projectile penetration [2, 3]. In this mode projectile material spreads along the target contact boundary since its strength is significantly lower than mechanical stress in the contact area. The projectile length is reducing to almost zero during the penetration (the projectile "wears away") [4, 5]. The analysis was carried out for rod-shaped projectiles made of high-density materials providing a highly effective penetration.

When a cylinder-shaped axissymmetrical projectile interacts with a target along its front surface normal, this continuum mechanical problem can be considered as a two-dimensional axissymmetrical problem. In a cylindrical coordinate system (r, z), both the motion and the state of the

deformable medium (of target and projectile materials) can be described by the following set of equations of the continuum mechanics [1].

Materials density ρ changes according to the law of mass conservation in the notation of calculus (continuity equation):

$$\frac{1}{\rho}\frac{d\rho}{dt} + \frac{\partial v_r}{\partial r} + \frac{v_r}{r} + \frac{\partial v_z}{\partial z} = 0$$

here v_r, v_z are radial and axial components of the material particle velocity.

Radial and axial accelerations of the material particles are defined according to the impulse law in the notation of calculus:

$$\rho\frac{dv_r}{dt} = \frac{\partial \sigma_r}{\partial r} + \frac{\sigma_r - \sigma_\theta}{r} + \frac{\partial \tau_{rz}}{\partial z};$$

$$\rho\frac{dv_z}{dt} = \frac{\partial \sigma_z}{\partial z} + \frac{\partial \tau_{rz}}{\partial r} + \frac{\tau_{rz}}{r},$$

here σ_r, σ_z, σ_θ τ_{rz} are normal and tangential components of the stress tensor.

Mechanical stresses due to the deformation of the target and projectile materials (metals) are calculated according to the model of the compressible elastoplastic medium. Strain rate tensor components $\dot{\varepsilon}_r, \dot{\varepsilon}_z, \dot{\varepsilon}_{rz}$, of the materials are expressed by velocity vector components derived from kinematic equations:

$$\dot{\varepsilon}_r = \frac{\partial v_r}{\partial r}; \quad \dot{\varepsilon}_z = \frac{\partial v_z}{\partial z}; \quad \dot{\varepsilon}_\theta = \frac{v_r}{r}; \quad \dot{\varepsilon}_{rz} = \frac{\partial v_z}{\partial r} + \frac{\partial v_r}{\partial z}.$$

Tension evolution of the materials which can undergo significant plastic deformations here is based on the incremental plasticity theory [1]. In this case the major equations of this theory (Prandtl—Reiss equations) are written in the form of the following differential equations:

$$\frac{d\,s_z}{d\,t} + 2G\dot{\lambda}s_z = 2G\left(\dot{\varepsilon}_z + \frac{1}{3\rho}\frac{d\rho}{dt}\right);$$

$$\frac{ds_r}{dt} + 2G\dot{\lambda}s_r = 2G\left(\dot{\varepsilon}_r + \frac{1}{3\rho}\frac{d\rho}{dt}\right);$$

$$\frac{ds_\theta}{dt} + 2G\dot{\lambda}s_\theta = 2G\left(\dot{\varepsilon}_\theta + \frac{1}{3\rho}\frac{d\rho}{dt}\right);$$

$$\frac{d\,\tau_{rz}}{dt} + 2G\dot{\lambda}\tau_{rz} = G\dot{\varepsilon}_{rz},$$

here s_z, s_r, s_θ are normal components of the stress tensor deviator, G is a medium shear modulus, $\dot{\lambda}$ is scalar factor defined by a specific capacity of

the plastic yield dA_p/dt and by the yield stress σ_Y as

$$\lambda = \frac{3}{2\sigma_Y^2} \frac{dA_p}{dt}.$$

A simplified method of Prandtl – Reiss [6] incremental plasticity equations can be useful while applying an approach of reducing the vector of the stress tensor deviator to the yield circle for solving elastoplastic medium mechanical problems. In accordance with this approach, the components of the stress tensor deviator were calculated assuming the elastic behavior of the material. The following set of equations was used:

$$\frac{ds_z}{dt} = 2G\left(\dot{\varepsilon}_z + \frac{1}{3\rho}\frac{d\rho}{dt}\right) + \delta_z;$$

$$\frac{ds_r}{dt} = 2G\left(\dot{\varepsilon}_r + \frac{1}{3\rho}\frac{d\rho}{dt}\right) + \delta_r;$$

$$\frac{ds_\theta}{dt} = 2G\left(\dot{\varepsilon}_\theta + \frac{1}{3\rho}\frac{d\rho}{dt}\right);$$

$$\frac{d\tau_{rz}}{dt} = G\dot{\varepsilon}_{rz} + \delta_{rz},$$

here δ_z, δ_z, δ_{rz} are corrections of the stress tensor deviator components connected to the rotation of a specified medium element as a rigid unit and calculated according to the following equations:

$$\delta_z = \tau_{rz}\left(\frac{\partial v_z}{\partial r} - \frac{\partial v_r}{\partial z}\right); \quad \delta_r = \tau_{rz}\left(\frac{\partial v_r}{\partial z} - \frac{\partial v_z}{\partial r}\right);$$

$$\delta_{rz} = \frac{1}{2}(s_z - s_r)\left(\frac{\partial v_r}{\partial z} - \frac{\partial v_z}{\partial r}\right).$$

Then both the Mises yield is checked. The stress tensor deviator components are corrected if required. An auxiliary function is calculated

$$J = 2\left(s_r^2 + s_z^2 + s_\theta^2 + 2\tau_{rz}^2\right).$$

In case the values of s_z, s_r, s_θ, τ_{rz}, which were calculated assuming material elastic behavior, conform to the condition $J > (2/3)\sigma Y_2$ (it corresponds to the plastic flow of the material), they are multiplied by $\sqrt{2/3(3J)}\sigma_Y$ [6] for correction.

With the use of the values s_z, s_r, s_θ, calculated according to the incremental plasticity and pressure p, normal components $\sigma_z = s_z - p$, $\sigma_r = s_r - p$, $\sigma_\theta = s_\theta - p$ of the stress tensor are calculated, these components are included in the equations of axial motion of the material particles.
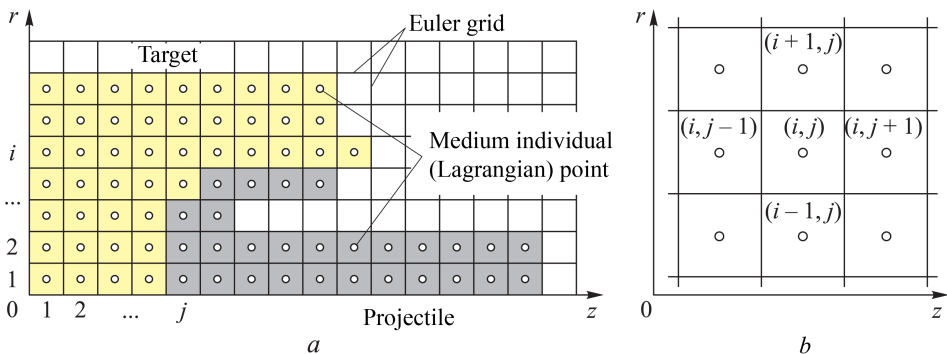
Fig. 1. Computational scheme of the free Lagrangian points method:
a — discretization of the computational area; b — finite-difference scheme template

Pressure inside the metals as a function of volumetric deformation (density ratio ρ/ρ_0) is often calculated by the barotropic equation [3]:

$$p = A\left((\rho/\rho_0)^n - 1\right), \qquad (1)$$

here ρ_0 is material density at normal conditions (at zero pressure); A, n are empirical constants of the material. When metal projectiles interact with the metal targets at velocities with the order of one to two kilometers per second, the influence of material internal energy on pressure can be neglected.

Boundary conditions of the problem in question (Fig. 1, a) are as follows. It is assumed that on the axis of symmetry ($r = 0$) there is no radial component of the medium particle velocity ($v_r = 0$). Mechanical stresses on the free surfaces of the target and projectile materials are assumed to be zero. On the contact surface of both the projectile and the target, normal and tangential stresses in the interacting materials must be equal to each other.

After setting the initial conditions it is assumed that the target material is at rest and is not disturbed (velocities and all components of the stress-strain state are zero). At the initial moment the projectile material is also assumed to be undisturbed (all components of the stress-strain state are zero). In addition to that the same velocity v_0 oriented along z axis is set at $t = 0$ for the whole volume of the projectile material.

For numerical solution to the formulated problem, a computational algorithm is used, which is based on the method of free Lagrangian points [7, 8].

The basic concept of the numerical method is as follows [9]. In the computational area, a fixed Euler mesh is introduced. It has orthogonal cells of the size Δ_r in the radial direction and Δ_z in the axial direction (see Fig. 1, a). Some individual (Lagrangian) points of the medium are placed into these Euler mesh cells, which are located inside the computational

field area occupied by the medium. The individual points have neither size nor mass. All parameters of the medium are defined at the points, such as radial and axial components of the velocity vector, density, and components of the stress tensor. Radial and axial coordinates characterize each point.

Each Euler mesh cell is individualized by a pair of integer numbers (i, j), here i is a cell number in the radial direction, j is a cell number in the axial direction (see Fig. 1, a).

The same pair of numbers is used as an index for all parameters of the medium in the individual (Lagrangian) point which is located inside this Euler cell (i, j) at this moment. For calculation of the parameters evolution in a Lagrangian point, which is located inside the Euler mesh cell (i, j), the parameters of Lagrangian points from four adjacent Euler cells are used. They are a lower cell $(i - 1, j)$, an upper cell $(i + 1, j)$, a right cell $(i, j + 1)$, and a left cell $(i, j - 1)$ (Fig. 1, b). If some of these Euler cells are empty (not occupied by the medium), they are considered to be occupied by dummy points having the same velocity vector components as the individual point at zero pressure. Introduction of the dummy Lagrangian points allows calculating the evolution of all individual points' parameters similarly regardless of the number of their adjacent points.

For instance, a new density value $\rho^*(i, j)$ (at the moment $t + \Delta t$) at the Lagrangian point located at the moment t inside the Euler mesh cell (i, j) is calculated by a differential analog of the continuity equation

$$\rho^*_{(i,j)} = \rho_{(i,j)} \left(1 - \Delta t \left(\frac{v_{r(i+1,j)} - v_{r(i-1,j)}}{r_{(i+1,j)} - r_{(i-1,j)}} + \right.\right.$$

$$\left.\left. + \frac{v_{r(i+1,j)} + v_{r(i-1,j)}}{r_{(i+1,j)} + r_{(i-1,j)}} + \frac{v_{z(i,j+1)} - v_{z(i,j-1)}}{z_{(i,j+1)} - z_{(i,j-1)}} \right)\right).$$

Similarly, all the other medium motions and state parameters at another time can be calculated by differential analogs of the corresponding equations.

Then, new radial and axial coordinates of the individual points are calculated

$$r^*_{(i,j)} = r_{(i,j)} + \Delta t \, v_{r(i,j)};$$

$$z^*_{(i,j)} = z_{(i,j)} + \Delta t \, v_{z(i,j)}.$$

These coordinates are used for redistribution of the individual points among the Euler mesh cells. For each individual point new indices, i and j, of the Euler cell are defined while the point is located at new time. Besides, if some Euler mesh cells contain several individual points, all these points are replaced by one point which has parameters averaged by parameters of

the "joined" points. The points on the boundary occupied by the medium (Euler cells containing these points have at least one empty cell among their adjacent cells) are excluded from this rule. If one Euler cell contains several individual points, one of which is a boundary point, only the boundary point is used for calculation and all the other points are excluded from the calculation.

After redistribution of the individual points among the cells of the Euler mesh the described computational procedure is repeated. An artificial viscosity [1] is introduced into the described computational scheme for continuous calculation of the shock waves. In case of the medium compression this viscosity gives a summand added to the hydrodynamic pressure acting at this point (a combination of linear and quadratic artificial viscosity is used).

Integration time step Δt is selected under the Current stability condition [1] and it meets the following inequation:

$$\Delta t < \min_{(i,j)} \frac{\Delta l}{c_{(i,j)} + \sqrt{v^2_{r(i,j)} + v^2_{z(i,j)}}},$$

here $c_{(i,j)}$ is speed of sound at Lagrangian points, Δl is least of the Euler mesh steps along the radial (Δr) and axial (Δz) coordinates (generally, the Euler mesh with square cells is used where $\Delta r = \Delta z$).

The described above computational algorithm is implemented in the numerical simulation software ERUDIT (Russian abbreviation for Heuristic Calculation of Ordered Motion of Individual Points) developed at Bauman Moscow State Technical University which was used in the presented research. Computational method described here was tested while solving a wide variety of explosive and impact continuous medium loading problems (as well as penetration problems) and showed positive results [10–12]. One of its advantages is the ability to calculate a motion of the continuous medium with large deformations without using specialized procedures of computational mesh regeneration.

In order to penetrate into the targets made of high-strength steel of a large width (more than 500 mm) elongated metal projectiles are used which have speed of approximately 1500 m/s. As it was mentioned above such projectiles penetrate into the targets in a hydrodynamic mode (when the projectile material spreads around the target contact area with the corresponding reduction of the projectile length during penetration). According to the hydrodynamic theory of penetration [2] the main factors affecting the target cavity depth are the following: a projectile length and its material density. Elongated projectiles made of the high density materials must be used for increasing a penetration depth. Such materials include

heavy alloys based on tungsten, nickel, and iron [13, 14]. Apart from possessing a high density (from 16.9 to 18.7 g/sm^3) these alloys feature a complex of other essential physical and mechanical properties which put them among major materials used for high penetrability projectiles production. These properties comprise a high plasticity (elongation up to 20 %), a high ultimate strength (above 1000 MPa), and a high yield strength (up to 900...1000 MPa).

All the above considered, a numerical analysis of penetration of the elongated projectiles made of tungsten-nickel-iron alloys proves important to conduct. It is necessary to have a dynamic compression curve of the alloy, which describes pressure inside the alloy as a function of its density. Compressibility of materials has certain effect on the penetration of elongated projectiles in a hydrodynamic mode [15, 16]. Therefore, a correct choice of $p(\rho)$ for the materials of both the target and projectile determines validity of the numerical simulation results and their correspondence to the real physical process.

An equation of dynamic compressibility for such multicomponent composition as a tungsten – nickel – iron alloy can be developed by applying the equations of compressibility for individual components [17]. Both assuming that total volumetric deformation of a multicomponent material is a sum of volumetric deformations of individual components and assuming equality of pressures in all components, interconnection between density and pressure in the tungsten – nickel – iron composition can be defined as follows:

$$\frac{\rho_0}{\rho} = \sum_{i=1}^{3} \alpha_i \left(1 + \frac{p}{A_i}\right)^{-1/n_i}, \qquad (2)$$

here values α_i describe phase composition of the heavy alloy and correspond to the volume density of tungsten, nickel, and iron (it is evident that the following relationship must be true: $\alpha_1 + \alpha_2 + \alpha_3 = 1$); A_i and n_i are parameters in the compressibility equations (1) for each individual component. When the phase composition is known, a standard density ρ_0 of a heavy alloy is defined as $\rho_0 = \alpha_1\rho_{10} + \alpha_2\rho_{20} + \alpha_3\rho_{30}$, here $\rho_{10} = 19350$ kg/m^3, $\rho_{20} = 8870$ kg/m^3, $\rho_{30} = 7850$ kg/m^3 are individual standard densities of tungsten, nickel, and iron respectively. Values of the empirical coefficients in the compressibility equations of these materials, which are used for obtaining the compressibility equation for the tungsten – nickel – iron high-density composition, are shown in the table [18].

When calculating we considered VNZh-90 alloy (Russian abbrevation for a W-Ni-Fe alloy) [14] with respective mass contents of tungsten, nickel, and iron $\mu_1 = 90$ %, $\mu_2 = 7$ %, $\mu_3 = 3$ % as the main material of the

Empirical coefficients in the compressibility equations of tungsten – nickel – iron heavy alloy components

Material	A, GPa	n
Tungsten	94.6	3.42
Nickel	45.3	4.507
Iron	19.5	5.642

elongated projectile. The density ρ_0 of this alloy was $\rho_0 = 17170 \text{ kg/m}^3$ at normal conditions. It was calculated by the formula

$$\frac{1}{\rho_0} = \frac{\mu_1}{\rho_{10}} + \frac{\mu_2}{\rho_{20}} + \frac{\mu_3}{\rho_{30}}.$$

Volume densities ρ_i in VNZh-90 alloy which are needed for drawing a curve of the alloy dynamic compression (2) were calculated by the equations $\alpha_i = \mu_i \rho_0 / \rho_{i0}$. They had the following values: $\alpha_1 = 79.9\,\%$ (for tungsten); $\alpha_2 = 13.5\,\%$ (for nickel); and $\alpha_3 = 6.6\,\%$ (for iron).

The obtained equation of the dynamic compressibility for VNZh-90 alloy in the form of equation (2) doesn't allow developing an explicit equation of the pressure p inside the material as a function of its density. It makes this equation impossible to use for a numerical simulation (as it is necessary to construct a special procedure for calculating pressure based on this relationship; it results in increasing the computational time significantly).

To solve this problem, equation (2) was approximated by the compressibility equation (1); the coefficients A and n were selected respectively. In order to determine these coefficients, the speed of sound in the alloy at normal conditions was calculated.

$$c_0 = \sqrt{\left.\frac{dp}{d\rho}\right|_{p=0}}.$$

When the function $p(\rho)$ is used in the form of equation (2), c_0 is calculated using the following equation:

$$\frac{1}{\rho_0 c_0^2} = \sum_{i=1}^{3} \frac{\alpha_i}{\rho_{i0} c_{i0}^2},$$

here c_{i0} — are the speeds of sound in the alloy components at normal conditions which are calculated on the basis of (1) as $c_{i0} = \sqrt{n_i A_i / \rho_{i0}}$. Calculation of the speed of sound inside VNZh-90 alloy at normal conditions resulted in a value $c_0 = 3950 \text{ m/s}$. On the other hand, the expression of c_0 which uses the approximating compressibility equation

$p(\rho)$ (1) can be written as $c_0 = \sqrt{nA/\rho_0}$ which allows linking the coefficients A and n: $A = \rho_0 c_0^2/n$. So the equation (1) can be rewritten as:

$$p = \frac{\rho_0 c_0^2}{n} \left[\left(\frac{\rho}{\rho_0} \right)^n - 1 \right],$$

where there is the only unknown coefficient n. This coefficient was selected in case if a deviation of equation (1) from compressibility equation (2) of the multicomponent material containing tungsten, nickel, and iron in the given ratio is minimal. A pressure range was considered from 0 to 40 GPa which overlapped the domain of pressures occurring during the material interactions at velocities of 1000...2000 m/s.

In the end, to perform these numerical computations the dynamic compressibility equation (1) with coefficients $A = 57.1$ GPa; $n = 4.7$ was used. The contrastive analysis of the different dynamic compressibility curves of the observed material showed that equation (1) with the given values of the coefficients resulted in the similar way as the ones obtained by equation (2) for a multicomponent medium.

The numerical computations were performed for a cylinder shaped projectile made of VNZh-90 alloy with the length of $l_0 = 500$ mm and a diameter of $d_0 = 24$ mm (elongation of $l_0/d_0 \approx 21$). The target was assumed to be made of steel with the strength corresponding to the steel targets of a medium hardness (a yield strength was set 1000 MPa). Dynamic compressibility of the steel target was defined by equation (1) with the coefficients $A = 19.5$ GPa; $n = 5.642$ [18]. Target thickness was 800 mm and its lateral size (diameter) was 320 mm.

While analyzing the impact of the projectile material strenght on the target penetration, its yield strength σ_Y was taken to be equal to 50; 500; 1000, and 1500 MPa.

Fig. 2 shows the final shapes of the cavities in the steel targets obtained during the penetration of the elongated rods made of VNZh-90 alloy with different yield strengths and the initial interaction velocity $v_0 = 1600$ m/s. The results
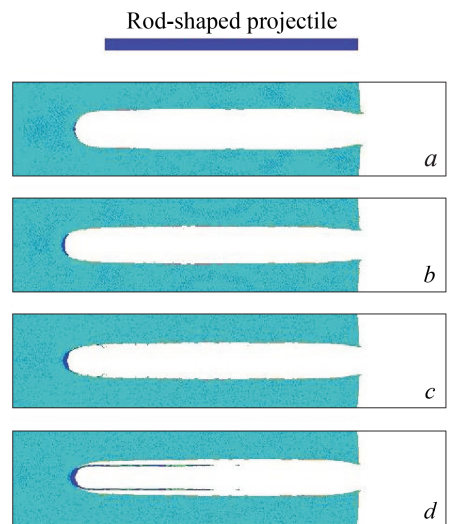

Рис. 2. Steel target cavity shape during the penetration of VNZh-90 alloy elongated projectiles with different yield strengths at initial interaction velocity of 1600 m/s:
$a - d - \sigma_Y = 50; 500; 1000; 1500$ MPa, respectively
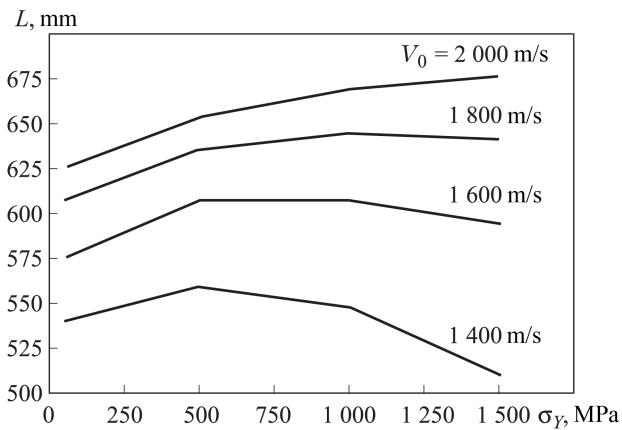
Fig. 3. Velocity and yield strength impact on the VNZh-90 alloy elongated projectile steel target penetration depth

obtained by varying the initial velocities of the projectiles are summarized in Fig. 3 by the curves linking penetration depth L (a cavity depth inside the target measured from initial position of its free surface) with the initial velocity v_0 of the projectile and its material yield strength σ_Y. Analysis of the given data shows that projectile material strength properties (its yield strength) produce relatively little effect on its penetration depth at the given interaction velocities. So at velocity $v_0 = 1400$ m/s the difference between the maximal and minimal penetrations for a yield strength σ_Y ranging from 50 to 1500 MPa is no more than 10 % (the maximal penetration is 560 mm, the minimal penetration is 510 mm). The higher the interaction velocity is the less the effect from the yield strength becomes. The penetration depth change, which is a function of the projectile material yield strength σ_Y at $v_0 = 2000$ m/s, is about 7 %.

It is of particular interest a "singular" effect of the projectile material strength on the penetration depth which becomes especially evident at a velocity $v_0 = 1400$ m/s (see Fig. 3). This "singularity" implies the existence of an extremum. It means that as the yield strength σY rises, the penetration depth increases at first, but then it starts decreasing. The above-mentioned behavior of the penetration depth L being a function of the projectile material yield strength remains unchanged at the initial interaction velocities of 1600 and 1800 m/s. Moreover, as the velocity increases a peak location shifts in the direction of higher σ_Y. At $v_0 = 2000$ m/s a cavity depth within the given range from 50 to 1500 MPa increases monotonically as σ_Y rises. However, it is evident that if the projectile material yield strength (above 1500 MPa) continues increasing, L must start decreasing.

At the velocity $v_0 = 1400$ m/s the penetration depth of the projectile with the minimum strength ($\sigma_Y = 50$ MPa) turns out to be higher than in

case of $\sigma_Y = 1500\,\text{MPa}$ ($L = 540\,\text{mm}$ vs. $L = 510\,\text{mm}$, Fig. 3). It is clear that this "singular" effect found during the numerical computations needs physical explanation. This explanation can be done in terms of energy. It is known that a volume of the cavity, which is formed in the target during the high-velocity penetration of the projectile, depends on its kinetic energy [19]. As it can be seen in Fig. 2, with the increase of the projectile material yield strength at a fixed velocity there is a certain decrease of the cavity lateral size (it evidently occurs due to some difficulties in the projectile material spreading in the lateral direction on the contact boundary with the target because of the strength forces). Decrease of the cavity lateral size under the condition of a fixed volume must lead to increase of the penetration depth. This fact seems to explain the initial increase of L along with the increase of the projectile material yield strength. The stronger projectile deforms less in the radial direction, which results in spending less energy for radial expansion of the cavity. Further decrease of the penetration depth along with the increase of the projectile material strength can be connected with the increase of the energy spent on the plastic deformation of the projectile itself.

It must be noted that the elongated projectile penetration model didn't account for the situation of possible destruction of both the projectile and target materials which can happen under the real conditions. However, this fact appears to have insignificant impact on the projectile penetration dependence on the projectile material strength. The destruction cannot immediately occur in the penetration area (in the projectile and target material contact area of a radial size, which corresponds to the projectile radius) since the materials are in the state of uniform compression in this area. Destruction may appear (and experimental data prove it) when the projectile material spreading over the penetration area in the radial direction takes the form of a thin film and its intensive plastic deformation almost stops. This film composition (whether it remains continuous or undergoes destruction) is of little significance considering its impact on the penetration.

Summing everything up it should be noted that the real values of σ_Y for the the VNZh-90 alloy (at the level of $1000\,\text{MPa}$) are close to optimal which provide the maximal penetration depth (see Fig. 3).

As it can be seen in Fig. 3, the projectile velocity has an impact on the penetration depth that is more significant than on the projectile material strength. The velocity of a projectile made of the VNZh-90 alloy with the yield strength of 1000 MPa increases from 1400 to $2000\,\text{m/s}$, which results in 12 mm cavity depth increase (from $L = 545\,\text{mm}$ to $L = 670\,\text{mm}$); it is approximately 23 %. As the velocity increases, a cavity lateral size increases considerably as well.

It must be noted that a hydrodynamic limit of the penetration depth (calculated according to the hydrodynamic penetration theory [2] using both the projectile length and its density – a target density ratio) for the VNZh-90 alloy projectile with the length of $l_0 = 500$ mm, in the case of a steel target is about 740 mm. Therefore, the penetration depth at $v_0 = 2000$ m/s is additionally about 10 % less than its hydrodynamic limit.

Fig. 4 shows the material density fields at different time, which illustrates the penetration of a steel target by the VNZh-90 alloy rod-shaped projectiles with the length of $l_0 = 500$ mm and a typical yield strength ($\sigma_Y = 1000$ MPa) at the initial velocities $v_0 = 1400$ m/s (Fig. 4, a) and $v_0 = 2000$ m/s (Fig. 4, b). The presented results prove that in both
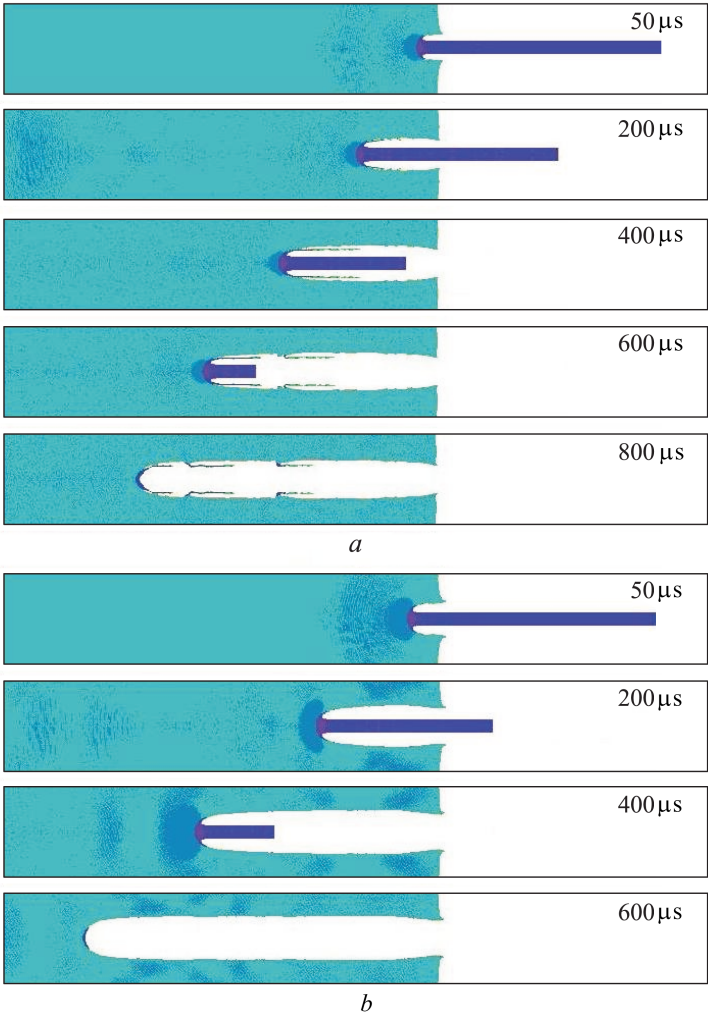

Fig. 4. Steel target penetration by the VNZh-90 alloy elongated projectiles with the yield strength of 1000 MPa at different initial velocities:
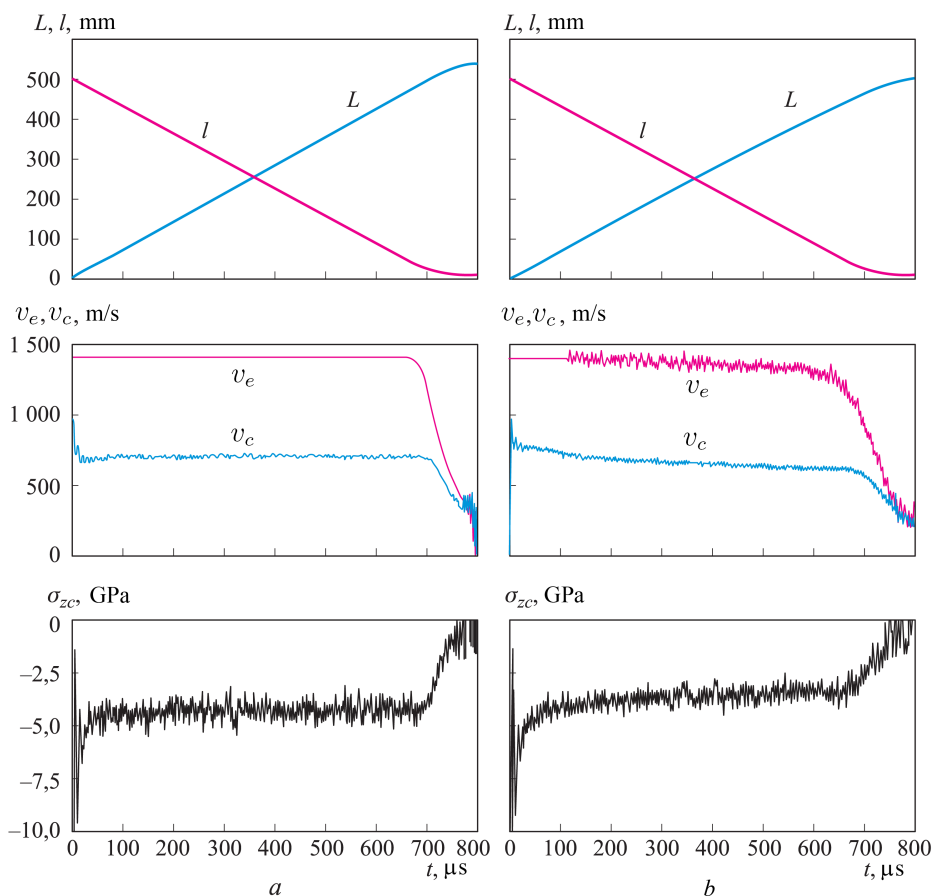$a - v_0 = 1400$ m/s; $b - v_0 = 2000$ m/s

Fig. 5. Change of the parameters during the steel target penetration by the VNZh-90 alloy rod with the yield strength of 50 MPa (*a*) and 1500 MPa (*b*) at the initial interaction velocity of 1400 m/s

cases a hydrodynamic penetration mode occurs when the projectiles "wear away" completely as a result of their material spreading along the contact boundary of the cavity formed in the target.

Fig. 5 and 6 illustrate the dynamical penetration of the VNZh-90 alloy elongated projectiles used in the computations. It is illustrated by a time ratio of the penetration depth L, a projectile current length l, a projectile trailing end velocity v_e, a penetration velocity v_c, and an axial stress σ_{zs} on the contact border of the target constructed for the following projectile initial velocities v_0 and yield strength σ_Y values: $v_0 = 1400$ m/s, $\sigma_Y = 50$ MPa (Fig. 5, *a*); $v_0 = 1400$ m/s, $\sigma_Y = 1500$ MPa (Fig. 5, *b*); $v_0 = 2000$ m/s, $\sigma_Y = 1000$ MPa (Fig. 6).

Comparison of the data in Fig. 5 shows a significant difference between a dynamical behavior of the penetration parameters for the projectile with a minimum strength ($\sigma_Y = 50$ MPa, see Fig. 5, *a*) and for a projectile with a very high strength ($\sigma_Y = 1500$ MPa, see Fig. 5, *b*) at the same initial velocity.
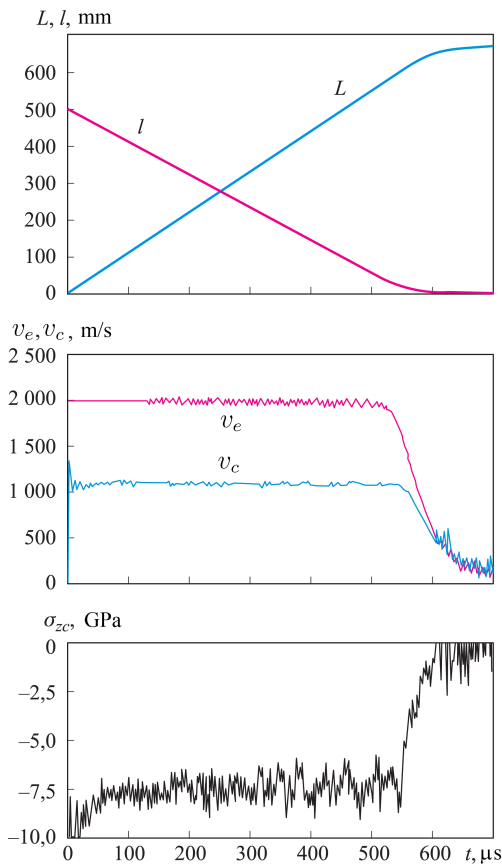
Fig. 6. Change of parameters during the steel target penetration of the VNZh-90 alloy rod with the yield strength of 1000 MPa at the initial interaction velocity of 2000 m/s

Both the projectile trailing end velocity v_e and the steel target contact boundary velocity v_c of a low strength projectile remain constant during the whole penetration process. Their values drop to zero only at the very moment when the projectile length reduces to the value close to its diameter (see Fig. 5, *a*). On the contrary, in the case of a high-strength projectile there is a visible reduction of the velocities v_e and v_c at the early stages of the process (see Fig. 5, *b*). This fact correlates with the Alekseyevsky – Tate rod-shaped projectile penetration model [4, 5]. Velocity reduction of the remaining part of the high-strength projectile during the penetration results in reducing contact stresses σ_{zc} while contacting with the target (see Fig. 5, *b*). For a low-strength projectile these stresses remain approximately constant up to the moment when the projectile length becomes zero (see Fig. 5, *a*). The performed analysis highlights physical factors, which cause a higher penetration effect when a projectile with the yield strength $\sigma_Y = 50$ MPa is used comparing to a projectile with the yield strength $\sigma_Y = 1500$ MPa at the interaction velocity $v_0 = 1400$ m/s.

When the projectile velocity rises up to $v_0 = 2000$ m/s, a rather high yield strength of the projectile material ($\sigma_Y = 1000$ MPa) does not cause any noticeable deceleration of the remaining part of the projectile (see Fig. 6). The penetration velocity v_0 — initial velocity v_0 ratio at $v_0 = 2000$ m/s turns out to be significantly higher than at $v_0 = 2000$ m/s, which apparently arises from the reduction of the target strength effect during the increase of the interaction velocity. Contact stress σ_{zc} at the target interface increases almost twofold (approximately from 4 up to 7,5 GPa) when the interaction velocity rises from 1400 to 2000 m/s.

In the both cases this stress is much higher than the yield strength of the projectile material which provides conditions for a hydrodynamic penetration mode.

In general, the results of the numerical computation show that the material strength of the elongated projectiles made of a high-density alloy has an insignificant impact on their penetration at the interaction velocities of 1500 m/s and higher. Therefore, it does not seem to require taking special measures for increasing material strength up to the maximal possible limit while developing the production process of the high-density rod-shaped projectiles. On the contrary, the analysis showns that a very high yield strength of the elongated projectile material may result even in a certain decrease of the projectile penetration.

According to the results of the numerical simulation, the dependence of the projectile penetration depth on its material yield strength is nonmonotonic and has a poorly defined extremum corresponding to the maximal penetration.

REFERENCES

[1] Babkin A.V., Kolpakov V.I., Okhitin V.N., Selivanov V.V. Prikladnaya mekhanika sploshnykh sred. V 3 t. T. 3. Chislennye metody v zadachakh fiziki vzryva i udara [Applied continuum mechanics. In 3 vol. Vol. 3. Numerical methods in problems of physics of explosion and shock]. Moscow, MGTU im. N.E. Baumana Publ., 2000. 516 p.
[2] Sagomonyan A.Ya. Pronikanie [Penetration]. Moscow, MGU Publ., 1974. 300 p.
[3] Fomin V.M., Gulidov A.I., Sapozhnikov G.A. Vysokoskorostnoe vzaimodeystvie tel [High-speed interaction of bodies]. Novosibirsk, Izd. SO RAN Publ., 1999. 600 p.
[4] Alekseevskiy V.P. On the penetration of the rod into the target at high velocity. *Fiz. Goreniya Vzryva* [Combust., Explos., Shock Waves], 1966, vol. 2, no. 2, pp. 99–106 (in Russ.).
[5] Tate A. A theory for the deceleration of long rods after impact. *J. Mech. Phys. Solids*, 1967, vol. 15, no. 6, pp. 387–399.

[6] Wilkins M.L. Alder B., Fernbach S., Retenberg M., eds. Calculation of elastic-plastic flow, methods of computational physics. New York, Academic Press, 1964. (Russ. Ed.: Uilkins M.L. Raschet uprugoplasticheskikh techeniy: Vychislitel'nye metody v gidrodinamike. Per. s angl. Moscow, Mir Publ., 1967, pp. 212–263.).

[7] Oran E.S., Boris J.P. Numerical simulation of reactive flow. 2nd Ed. Cambridge Uni. Press, Naval Research Laboratory Publ., 2001. 522 p. (Russ. Ed.: Oran E., Boris Dzh. Chislennoe modelirovanie reagiruyushchikh potokov. Per. s angl. Moscow, Mir Publ., 1990. 660 p.).

[8] Fedorov S.V. On the possibility of "cutoff" of the leading high-velocity portion of the metal jet in the explosion of a shaped charge in the axial magnetic field. *Boepripasy i vysokoenergeticheskie kondensirovannye sistemy* [Explosives and high energy condensed system], 2008, no. 2, pp. 73–80 (in Russ.).

[9] Veldanov V.A., Markov V.A., Pusev V.I., Ruchko A.M., Sotskiy M.Yu., Fedorov S.V. Computation of nondeformable striker penetration into low-strength obstacles using piezoelectric accelerometry data. *Zh. Tekh. Fiz.* [Tech. Phys. The Russ. J. Appl. Phys.], 2011, vol. 56, iss. 7, pp. 94–104 (in Russ.).

[10] Fedorov S.V., Veldanov V.A. Numerical simulation of cavity formation in soil by a flux of high-speed metallic penetrators. *Zh. Tekh. Fiz.* [Tech. Phys. The Russ. J. Appl. Phys.], 2006, vol. 76, iss. 7, pp. 134–137 (in Russ.).

[11] Fedorov S.V. By definition the penetration depth of mushy projectiles at hypervelocity interaction. *Zh. Tekh. Fiz.* [Tech. Phys. The Russ. J. Appl. Phys.], 2007, vol. 77, iss. 10, pp. 131–134 (in Russ.).

[12] Fedorov S.V., Veldanov V.A. Determining of the dimension of a cavity in water behind a fast-moving cylindrical body. *Zh. Tekh. Fiz.* [Tech. Phys. The Russ. J. Appl. Phys.], 2013, vol. 83, iss. 2, pp. 15–20 (in Russ.).

[13] Magness L.S., Kapoor D. Tungsten composite materials with alternative matrices for ballistic applications. *Proc. of the Fifth Intern. Conf. on Tungsten: "Hard Metals and Refractory Alloys".* Princeton, New Jersey, 2000, pp. 15–23.

[14] Povarova K.B., Makarov P.V., Ratner A.D., Zavarzina E.K., Volkov K.V. VNZh-90 type heavy alloys. 1. Effect of alloying and conditions of tungsten powders production of structure and properties of sintered alloys. *Metally* [Russ. Metall. (Engl. Transl.)], 2002, no. 4, pp. 39–48 (in Russ.).

[15] Zlatin N.A. O roli szhimaemosti v protsesse dinamicheskogo deformirovaniya plastichnykh tel. Nekotorye problemy prochnosti tverdogo tela [On the role of compressibility in the process of dynamic deformation of plastic bodies. In book "Some problems of the strength of solids"]. Moscow–Leningrad, AN SSSR Publ., 1959, pp. 222–229.

[16] Fedorov S.V., Bayanova Ya.M. Penetration of long strikers under hydrodynamic conditions with allowance for the material compressibility. *Zh. Tekh. Fiz.* [Tech. Phys. The Russ. J. Appl. Phys.], 2011, vol. 56, iss. 9, pp. 45–51 (in Russ.).

[17] Nigmatulin R.I. Dinamika mnogofaznykh sred [Dynamics of multiphase media. Pt. 1]. Moscow, Nauka Publ., 1987. 464 p.

[18] Zhernokletov M.V., eds. Metody issledovaniya svoystv materialov pri intensivnykh dinamicheskikh nagruzkakh [Methods for studying the properties of materials under intense dynamic loads]. Sarov, FGUP "RFYaTs-VNIIEF" Publ., 2005. 428 p.

[19] Kinslow R. (Ed.), High velocity impact phenomena. New York, Academic Press, 1970. 529 p. (Russ. Ed.: Nikolaevskiy V.N. ed. Vysokoskorostnye udarnye yavleniya. Per. s angl. Moscow, Mir Publ., 1973. 538 p.).

Contributors

Fedorov S.V. — Senior Lecture, Department of High Precision Airborne Devices, Bauman Moscow State Technical University, author of over 250 research publications in the fields of physics of explosion and high velocity impact.
Bauman Moscow State Technical University, ul. 2-ya Baumanskaya 5, Moscow, 105005 Russian Federation.

Veldanov V.A. — Ph.D. (Eng.), Associate Professor of Engineering, Department of High-Precision Flying Vehicles, Bauman Moscow State Technical University, author of over 230 research publications in the fields of ultimate ballistics and mechanics of deformable solid body.
Bauman Moscow State Technical University, ul. 2-ya Baumanskaya 5, Moscow, 105005 Russian Federation.

Smirnov V.E. — D.Sc. (Eng.), Professor of Engineering, Director of the Federal State-Funded Institution of Science Mechanical Engineering Research Institute, author of over 250 publications in the fields of ballistics and mechanics of deformable solid body.
Federal State-Funded Institution of Science Mechanical Engineering Research Institute, Leningradskoe shosse 58, Moscow, 105005 Russian Federation.

The translation of this article from Russian into English is done by Komissarov Aleksandr Igorevich, an engineer, a Ph.D. student the Department of Special Machinery, Bauman Moscow State Technical University under the general editorship of N.N. Nikolaeva, Ph.D. (Philol.), Associate Professor Linguistics Department, Bauman Moscow State Technical University.